Earth and Planetary Science Letters 388 (2014) 81–91

Contents lists available at ScienceDirect

Earth and Planetary Science Letters

www.elsevier.com/locate/epsl

Regulation of atmospheric oxygen during the Proterozoic

Thomas A. Laakso *, Daniel P. Schrag

Department of Earth and Planetary Sciences, Harvard University, Cambridge, MA 02138, USA

ARTICLE INFO

Article history:
Received 5 March 2013
Received in revised form 23 October 2013
Accepted 22 November 2013
Available online 18 December 2013
Editor: J. Lynch-Stieglitz

Keywords:
atmospheric oxygen
Proterozoic
phosphorus
iron

ABSTRACT

Many studies suggest that oxygen has remained near modern levels throughout the Phanerozoic, but was much less abundant from the "Great Oxygenation Event" around 2.4 Ga until the late Neoproterozoic around 600 Ma (Kump, 2008). Using a simple model, we show that the maintenance of atmospheric pO_2 at ~1% of present atmospheric levels (PAL) is inconsistent with modern biogeochemical cycling of carbon, sulfur and iron unless new feedbacks are included. Low oxygen conditions are stable in our model if the flux of phosphorus to the oceans was greatly reduced during the Proterozoic. We propose a mechanism to reduce this flux through the scavenging of phosphate ions with an "iron trap" driven by greater surface mobility of ferrous iron in a low pO_2 world. Incorporating this feedback leads to two stable equilibria for atmospheric oxygen, the first quantitative hypothesis to explain both Proterozoic and Phanerozoic O_2 concentrations.

1. Introduction

Atmospheric oxygen has passed through three broad plateaus in earth history (Kump, 2008). Mass-independent sulfur isotopes show that it was negligibly low during the Archean, rising abruptly around 2.4 Ga (Pavlov and Kasting, 2000). Paleosols (Rye and Holland, 1998), pyrite and uraninite grains (Holland, 1984), sulfur isotopes (Canfield and Teske, 1996), and widespread ferrous and euxinic basins (Poulton and Canfield, 2011) point to a moderately oxygenated Proterozoic, likely 1–10% PAL (Kump, 2008). Though pO_2 may have varied between these bounds through the Proterozoic, the appearance of large multicellular animals and large colonial algae supports a second rise in O_2 near the end of the Neoproterozoic (Anbar and Knoll, 2002), and the charcoal record requires at least 60% PAL since the Silurian (Scott and Glasspool, 2006). The two major oxidation events may have been complex oscillations in pO_2 (e.g. Anbar et al., 2007; Dahl et al., 2010), but the associated changes in the proxy record are abrupt compared to the length of the intervening periods. At hundreds of millions of years, this stability time scale is much greater than the residence times of redox-sensitive species, so the oxygen system must have been in several different steady states over geological history.

Much research has been devoted to the "Great Oxidation Event" of 2.4 Ga and the second oxidation in the terminal Proterozoic. These events have been attributed to any number of drivers. For the late Archean, these include abrupt overturning of a redox-stratified mantle (Kump et al., 2001), rapid hydrogen escape (Catling et al., 2001), or a change from more reducing submarine volcanism to more oxidized subaerial outgassing (Kump and Barley, 2007); for the late Proterozoic, the evolution of biological ballast (Logan et al., 1995), more active clay formation (Kennedy et al., 2006), or a perturbation related to the Snowball glaciation (Hoffman and Schrag, 2002).

Unfortunately, it is difficult to evaluate these hypotheses given our incomplete understanding of redox dynamics. The result of a perturbation or a change in geochemical cycling is only meaningful in the context of a dynamical system, which dictates the steady state values of pO_2 and the feedbacks that maintain them. To understand the oxygenation events and any transient oscillations, it is therefore necessary to understand the mechanisms underlying the long periods of stability in the Archean, Proterozoic and Phanerozoic. Goldblatt et al. (2006), for example, have suggested a model for bistability around the Great Oxidation Event, based on Archean photochemistry. In this study we use a simple model of ocean-atmosphere electron cycling to explore the feedbacks that can produce a two-state redox system corresponding to the Proterozoic and Phanerozoic.

Previous work on redox dynamics has mostly focused on the stability of the Phanerozoic atmosphere. Some models for past O_2 levels avoid the need for explicit feedbacks by using constraints from carbon isotope variations in marine carbonate, assumed to represent fluctuations in the burial of organic carbon relative to calcium carbonate (Berner, 2006). Other studies have explored the dynamical stability of the Phanerozoic using different negative feedbacks, particularly an oxygen-dependent weathering rate for reduced minerals (Kump and Garrels, 1986; Berner and Canfield, 1989; Lasaga and Ohmoto, 2002; Bergman et al., 2004). Oxygen-dependent burial efficiencies for organic carbon and sulfide have also been proposed (Kump and Garrels, 1986;

* Corresponding author. Tel.: +1 978 501 4379.
E-mail address: laakso@fas.harvard.edu (T.A. Laakso).

0012-821X/$ – see front matter
http://dx.doi.org/10.1016/j.epsl.2013.11.049

Berner and Canfield, 1989; Lasaga and Ohmoto, 2002). One study has investigated the stability of low-oxygen Proterozoic conditions (Fennel et al., 2005), but their model explicitly excluded the negative feedbacks known from the Phanerozoic work.

The series of feedbacks referenced above, when taken together, make it impossible to maintain very low pO_2, as low O_2 leads to higher organic carbon burial and the inevitable build-up of oxygen. Stabilizing O_2 at both high Phanerozoic levels *and* low Proterozoic levels requires either a slowly evolving external forcing, or a new feedback, previously undescribed. Rather than proposing a particular hypothesis, we build a model tuned to present-day conditions, and explore the sensitivity of its stable pO_2 level to different changes in the model parameters. By identifying those changes that can produce stable, Proterozoic-like conditions, we aim to narrow the list of geochemical processes that might host the forcing or feedbacks that allow for a two-state system.

2. Model

Our model couples the carbon, iron and sulfur cycles through first-order chemical reactions in a two-layer, phosphorus-limited (Tyrrell, 1999) ocean. The time-dependent equations are given Table 1, and the flux parameterizations discussed below are summarized in Table 2. The values of the model constants and the integration procedure are given in the Supplementary Material. The Phanerozoic equilibrium model is shown in Figure S1. This state was tuned to reproduce major electron fluxes, resulting in equilibrium pO_2 at 1.1 PAL.

2.1. Primary production and export

Primary production (NPP) and all subsequent organic cycling occurs at a fixed C:P Redfield ratio (r) of 106:1. Production proceeds to quantitative uptake (Sarmiento and Gruber, 2006) of phosphorus in the upper ocean layer during each time step. Production remaining after respiration, adsorption, and burial in shallow water sediments is exported to deep waters (EP).

2.2. Water-column remineralization

Remineralization in the water column is modeled as oxic respiration (R_{wc}) in the presence of oxygen, and sulfate reduction (S_{wc}) otherwise. Sulfate reduction rates are observed to follow Michaelis–Menten kinetics (e.g. Ingvorsen et al., 1984); our model uses a linear approximation. This results in a mineralization rate that is somewhat over-sensitive to sulfate levels above the Michaelis constant of ~200 μM SO_4^{2-} (Ingvorsen et al., 1984), though linearized behavior is a good approximation far from this value. We repeated our analysis using a Michaelis–Menten parameterization, and the basic results are not affected. Both modes of respiration are therefore modeled as linear in the concentration of the appropriate electron acceptor, [O_2] or [SO_4^{2-}], and in [C_{org}].

2.3. Organic carbon deposition

Organic carbon is deposited on the seafloor by two processes: ballasting (Armstrong et al., 2002) and unassisted sinking. The ballasted flux (B_a) is proportional to bulk sediment delivery (W_a) assuming a monolayer organic coat (Hedges and Keil, 1995), and to the availability of fresh organic material, represented by NPP. Organic ballast may be inappropriate for modeling the Proterozoic (Logan et al., 1995); sensitivity to this term is explored in Section 4.3.1. Unballasted sinking (B_C) is proportional to the unadsorbed, unrespired organic carbon concentration. This burial also scales with riverine nutrient inputs, such that when river delivery accounts for a larger fraction of new production, deposition under shallow waters increases at the expense of export. Details are given in Tables 2 and Table S1.

2.4. Sedimentary remineralization

Remineralization of organic carbon in the sediment includes oxic respiration (R_{sd}) and sulfate reduction (S_{sd}). Both processes are modeled as first order with oxidant concentration in the overlying water. The existence of such an "oxygen effect" has been controversial (Cowie et al., 1995; Hedges et al., 1999); detailed analysis of this parameterization is presented in Section 4.4.1.

The rate constant for sulfate reduction is modulated by a factor β, which scales linearly with the "lability" of carbon reaching the sulfate reduction zone, defined here as $(R_{sd} + R_{wc} + S_{wc})/\text{NPP}$. This increases the reduction rate when sulfate reducers have access to less degraded organic matter (Westrich and Berner, 1984).

2.5. Remineralization by other electron acceptors

Other electron acceptors are not included in the model as they are quantitatively much less important than oxygen and sulfur. Denitrification today is only a few percent of O_2 consumption (Canfield, 1993; DeVries, 2012). Iron and manganese are the dominant electron acceptors in some sedimentary environments, but in these cases the flux of metals to the sediment is an order of magnitude smaller than the reduction of those metals, requiring continuous reoxidation by more abundant species such as oxygen and sulfate (e.g. Wang and Van Cappellen, 1996). Globally, the modern fluxes of sulfate and highly reactive iron to the oceans are ~4 Tmol yr^{-1} (Elderfield and Schultz, 1996; Poulton and Raiswell, 2002), meaning sulfate can potentially oxidize eight times more organic carbon than iron. Even total titration of sulfur as FeS_2 in an anoxic ocean (Poulton and Canfield, 2011) requires only one electron out of every fifteen to be donated to iron.

Methanogenesis remineralizes about ten times less carbon globally than does sulfate reduction (Canfield, 1993). Some have argued methanogenesis is more important in the absence of other electron acceptors (Wang and Van Cappellen, 1996), an idea that has been invoked to model the Archean with burial efficiencies identical to today (Habicht et al., 2002). However, in Black Sea sediment cores only 0.3% of NPP is degraded via methanogenesis, compared to 4% via sulfate reduction (Jorgensen et al., 2001; Arthur et al., 1994), a ratio typical of oxic marine sediments despite burial efficiencies far above the global average (Arthur et al., 1994; Muller-Karger, 2005). In the sulfate-limited sediments of Cape Lookout Bight, methanogenesis accounts for a larger portion of anaerobic metabolism (Capone and Kiene, 1988), but still degrades less than ten percent of organic carbon reaching the sediment (Martens and Klump, 1984). At these scales, methanogenesis is negligible: our results are not affected if we include methane formation at a constant 1.3 Tmol C yr^{-1}, 10% of modern sulfate reduction.

Recently Crowe et al. (2011) reported that ~85% of primary production in ferruginous Lake Matano is degraded via methanogenesis, based on a methane flux through the pycnocline calculated from an assumed value for a diffusion coefficient. If exported organic matter is consumed primarily by methanogens, the CO_2 produced at depth should be enriched in ^{13}C to balance the production of methane. However, Crowe et al. report deep water $\sum CO_2 \delta^{13}C$ that is 1‰ depleted relative to surface waters, implying that methane production account for a much smaller fraction of organic matter degradation.

Table 1
Time-dependent evolution of the prognostic variables. a: atmosphere; s: shallow ocean; d: deep ocean. M is the volume of an ocean box.

$\frac{d}{dt}(O_2)_a = -W_C - \frac{15}{8}W_{pyr}$
$\frac{d}{dt}[O_2]_s M_s = -(R_{wc}) - 2Q + NPP$
$\frac{d}{dt}[O_2]_d M_d = -(R_{wc}) - 2Q$
$\frac{d}{dt}[SO_4^{2-}]_s M_s = Q - (S_{wc} + S_{sd}) - B_{S_{ox}} - \frac{1}{16}B_{pyr} + W_S$
$\frac{d}{dt}[SO_4^{2-}]_d M_d = Q - (S_{wc} + S_{sd}) - B_{S_{ox}} - \frac{1}{16}B_{pyr} - H_{S_{ox}}$
$\frac{d}{dt}[S^{2-}]_s M_s = -Q + (S_{wc} + S_{sd}) - \frac{15}{16}B_{pyr}$
$\frac{d}{dt}[S^{2-}]_d M_d = -Q + (S_{wc} + S_{sd}) - \frac{15}{16}B_{pyr} + H_{S_{rd}}$
$\frac{d}{dt}[C_{org}]_s M_s = -(R_{wc} + 2S_{wc}) - (B_a + B_C) + NPP - EP$
$\frac{d}{dt}[C_{org}]_d M_d = -(R_{wc} + 2S_{wc}) - (B_a + B_C) + EP$
$\frac{d}{dt}[PO_4^{3-}]_s M_s = \frac{1}{r}(R_{wc} + 2S_{wc}) - B_P + Y + \frac{1}{r}NPP + W_P$
$\frac{d}{dt}[PO_4^{3-}]_d M_d = \frac{1}{r}(R_{wc} + 2S_{wc}) - B_P$
$\frac{d}{dt}(C_{inorg})_s = (R_{wc} + R_{sd}) + 2(S_{wc} + S_{sd}) + V_C - B_{CO_3} + W_{CO_3} + W_C - NPP$
$\frac{d}{dt}(C_{inorg})_d = (R_{wc} + R_{sd}) + 2(S_{wc} + S_{sd}) + V_C - B_{CO_3}$
$\frac{d}{dt}[Ca^{2+}]_s M_s = -B_{CO_3} + W_{Ca}$
$\frac{d}{dt}[Ca^{2+}]_d M_d = -B_{CO_3}$

Table 2
Flux parameterizations. Values for the rate constants (k) and water mass volumes (M) vary between deep (d) and shallow (s) waters, but subscripts are not given here unless needed. Parameter values are given in Tables S1–S3. Note: $[C_{org}]$ includes net primary production and excludes adsorbed carbon from the current time step.

Process	Parameterization	mol yr^{-1}
Net primary production	$NPP = r[PO_4^{3-}]_s M_s$	C
Oxic respiration, water col.	$R_{wc} = k_0[O_2][C_{org}]M$	C
Sulfate reduction, water col.	$S_{wc} = k_1[SO_4^{2-}][C_{org}]M$	S
Sulfide oxidation	$Q = k_2[O_2][S^{2-}]M$	S
Gross burial of organic C	$B_C = \alpha k_3([C_{org}]M - (R_{sd} - 2S_{wc})) + B_a$	C
Adsorption of organic C	$B_a = k_4 W_a \cdots NPP$	C
Oxic respiration, sediment	$R_{sd} = k_5[O_2]M$	C
Sulfate reduction, sediment	$S_{sd} = \beta k_6[SO_4^{2-}]M$	S
Pyrite burial	$B_{pyr} = \gamma S_{sd}$	S
Sulfate burial	$B_{S_{ox}} = k_7[SO_4^{2-}]M$	S
Phosphorus scavenging	$B_P = k_8[PO_4^{3-}]M$	P
Phosphorus regeneration	$Y = \delta(R_{sd} + 2S_{sd})/r$	P
Weathering, organic C	$W_C = k_9(pO_2)^{1/2}$	O_2
Weathering, phosphorus	$W_P = \omega W_{ap} + f_b W_C/r$	P
Weathering, crust Fe^{2+}	$W_{Fe} = k_{10}[O_2]_d M_d$	Fe

2.6. Sulfide burial and oxidation

Sulfide produced during sulfate reduction is either oxidized or buried as pyrite (B_{pyr}). Pyrite burial is set to an oxygen-dependent fraction (γ) of the sulfide generated during sulfate reduction (Berner and Westrich, 1985). Iron limitation may be an important control, but we cannot include this effect without explicitly incorporating the iron cycle. The remaining sulfide diffuses from the sediment. For simplicity, the same pyritization fraction is applied to sulfate reduction in the water column. Aqueous sulfide can be oxidized to sulfate by O_2, with the flux (Q) first order in both species (Millero et al., 1987a).

2.7. Sulfate burial

Burial of sulfate minerals (gypsum, anhydrite, CAS) is lumped into one term (B_{Sox}) proportional to sulfate concentration. Actual deposition likely occurs during large evaporative events (e.g. Halevy et al., 2012). Our parameterization represents an average over many such events, with the assumption that total sulfate in an average evaporative basin must vary with ocean sulfate concentration. This smoothed burial flux is tuned to produce the 2:3 ratio of pyrite:sulfate burial required by isotopic mass balance (Canfield, 2004).

2.8. Sedimentary phosphorus cycling

Phosphorus released to pore waters during organic matter oxidation (R_{sd}, S_{sd}) can diffuse back into the water column. The diffusive flux (Y) is influenced by adsorption onto iron oxides (Shaffer, 1986; Sundby et al., 1992), which depresses phosphate concentrations above the iron redox front. Because the depth of this front depends on oxygen penetration depth, P diffusion should fall with rising oxygen. Therefore, we allow an oxygen-dependent fraction (δ) of remineralized P to diffuse from the sediment. Alternative parameterizations, such as preferential remineralization of organic P (Van Cappellen and Ingall, 1994), are considered in Section 4.4.2.

2.9. Weathering, volcanic, and hydrothermal fluxes

Weathering of bulk sediment (W_a), carbonates (W_{CO_3}), total calcium (W_{Ca}), and apatite (W_{ap}) all scale with a factor (ω) calculated from pCO_2 and temperature according to Walker et al. (1981). Temperature is calculated from pCO_2 by assuming a climate sensitivity of 3 K per doubling around 288 K at 280 ppm.

Phosphorus weathering (W_P) is the sum of apatite (W_{ap}) and organic phosphorus (W_C) weathering. Only a fraction (f_b) of remineralized organic P is considered to be non-detrital and thus biologically available (Froelich, 1988). Organic carbon weathering scales with the square root of pO_2 (Chang and Berner, 1999).

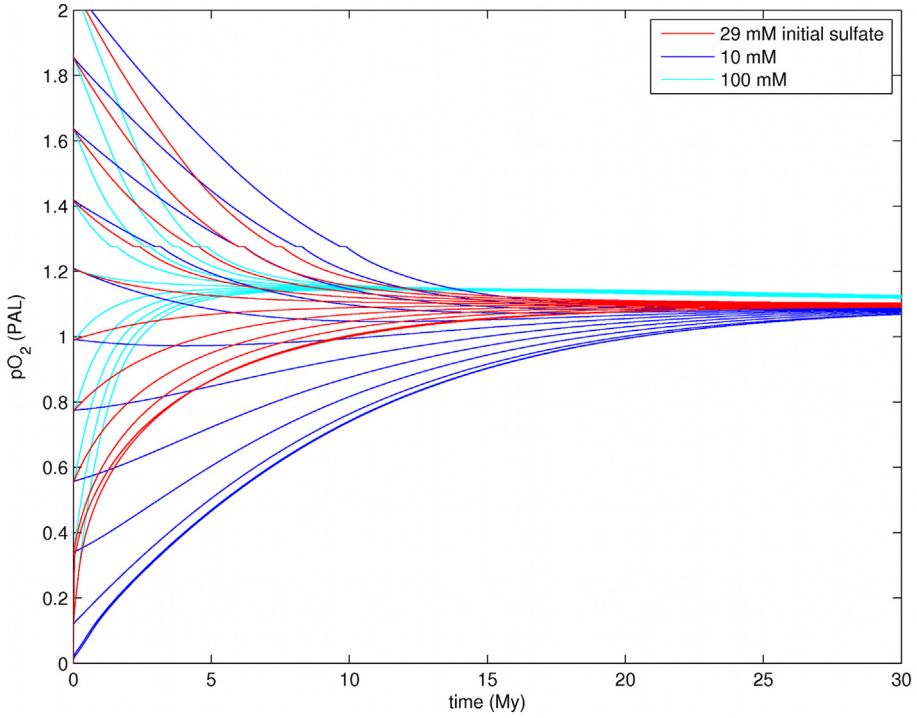

Fig. 1. Evolution of pO_2 after initializing the model with oxygen between 0 and 2 PAL, and sulfate between 10 and 100 mM.

Weathering of pyrite is a constant, reflecting exposure limited oxidation as inferred from the disappearance of detrital FeS_2 after the Archean (Holland, 1984).

Hydrothermal and volcanic fluxes are constants in the model. These include hydrothermal sulfate uptake and sulfide release, and volcanic carbon outgassing.

2.10. Calcite precipitation and dissolution

Calcite saturation state is fixed in the ocean, requiring computation of carbonate ion concentration from total carbon and alkalinity. Alkalinity varies from its modern day value based on variations in calcium. Given alkalinity and total carbon values, temperature-specific carbonate speciation is calculated, and precipitation of calcite is scaled to maintain saturation. Equilibrium carbonate speciation is recalculated, providing pCO_2. The details of this calculation are given in the Supplementary Material.

2.11. Mixing and ocean-atmosphere equilibrium

The mixing flux (F_X) for species y is calculated from $X([y]_s - [y]_d)$, with water exchange rate X (30). Oxygen is distributed between the atmosphere and surface ocean according to a partitioning constant η derived from Henry's constant. The details of these calculations are given in the Supplementary Material.

3. Results

3.1. pO_2 equilibria

There is only one equilibrium O_2 concentration in the model. For initial oxygen levels between zero and two times PAL, and with a range of initial sulfate (1–100 mM), organic carbon, and phosphate (0–3 μM) concentrations, the simulations return to modern pO_2 levels within 50 million years (Fig. 1).

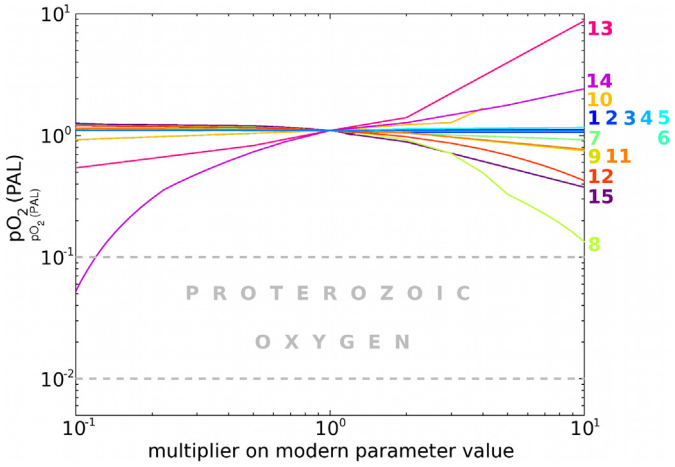

Fig. 2. Sensitivity of steady-state pO_2 to various model parameters. Each curve shows the sensitivity to a given parameter: 1: rate constant (RC) for organic carbon deposition (k_3), 2: water-column oxic respiration RC (k_0), 3: ballasting RC (k_4), 4: inorganic P deposition RC (k_8), 5: sediment sulfate reduction RC (k_6), 6: pyrite burial fraction intercept (γ at $[O_2] = 0$), 7: sulfate burial RC (k_7), 8: pyrite weathering (W_{pyr}), 9: organic carbon weathering RC (k_9), 10: P regeneration fraction (fixed δ for all $[O_2]$), 11: oxidation of ocean crust RC (k_{10}), 12: hydrothermal sulfide flux ($H_{S_{rd}}$), 13: volcanic outgassing (V_C), 14: riverine phosphorus flux (W_P), 15: sediment oxic respiration RC (k_5).

3.2. Sensitivity of the pO_2 equilibrium

The value of this sole equilibrium is remarkably insensitive to the model parameters (Fig. 2). We ran a sensitivity test over two orders of magnitude variation in each of the major model parameters. For each parameter, we describe in detail only the simulation that produces the largest reduction in pO_2. The full sensitivity results are shown in Fig. 2. Within the range tested, only a reduction in the phosphorus input flux can drive pO_2 to less than 0.1 PAL.

3.2.1. Sensitivity to water column carbon cycling

Deposition of organic carbon on the seafloor is modeled as proportional to organic carbon concentrations in the water column. Variations in the rate constant, representing changes in the sinking rate of particles, have no impact on oxygen: equilibrium pO_2 is 1.1 PAL after a ten-fold increase in the rate constant.

The acceleration in carbon deposition strips average P concentrations to 10 nM. Primary productivity falls in response, from $\sim$3000 Tmol C yr^{-1} to 300, such that the downward organic flux of P once again balances inputs. Total organic flux to the sediment, and hence the oxygen budget and pO_2, are unchanged.

Water column respiration rate is first-order in both oxygen and organic carbon concentration. pO_2 remains at 1.1 PAL for two orders-of-magnitude variation in the rate constant. A ten-fold decrease, representing much less labile organic carbon, reduces the efficiency of water-column remineralization from over 99% to about 70%. Phosphate concentrations plunge as the unremineralized organic P is buried. Production falls to 150 Tmol C yr^{-1}, such that the efficient export of a small, recalcitrant organic pool balances nutrient inputs. Again, balancing nutrient fluxes in a phosphorus-limited ocean guarantees that the organic flux to the sediment, and hence the oxygen budget, does not change.

3.2.2. Sensitivity to inorganic nutrient scavenging

We model the small inorganic deposition of phosphorus as first-order in phosphate concentrations. pO_2 falls to 0.7 PAL if the rate constant is increased by a factor of 10^4. The additional scavenging draws down P concentrations, slowing adsorption such that inorganic deposition itself grows by only a factor of 10^3, to 40% of the total shuttle. The reduction in nutrient supply slows productivity, reducing organic deposition by 9 Tmol C yr^{-1}, at which point the combined P sink again balances inputs. pO_2 falls in response, slowing sedimentary respiration until the fraction of organic carbon surviving diagenesis becomes large enough to compensate for the smaller gross flux, re-establishing redox equilibrium.

3.2.3. Sensitivity to sedimentary oxic respiration

Oxic respiration in the sediments is modeled as first order in the oxygen concentration of the overlying water column. A ten-fold increase in this rate constant drives pO_2 to 0.4 PAL. The increased rate of respiration means less efficient organic burial at a given oxygen level, i.e. a smaller fraction of gross organic deposition is ultimately buried. The oxygen source is thus reduced and pO_2 falls, slowing respiration and raising burial efficiency until the oxygen source again balances oxygen sinks. The model's linear dynamics suggest a ten-fold increase in the rate constant should be balanced by oxygen at 0.1 PAL; however, the response is damped to 0.4 PAL by three negative feedbacks.

First, pyrite burial efficiency scales with oxygen concentration. Decreases in O_2 therefore drive larger changes in the oxygen source than expected from the dynamics of organic carbon alone: after the ten-fold increase in the oxic respiration rate constant, pyrite burial increases by 60%.

Second, the fraction of pore water P regenerated to the water column falls off with the overlying oxygen concentration. In the simulation with high respiration rate constant, retention of pore water P decreases from 75% to 50%, driving up primary production and organic deposition to the sediment. The additional organic flux is effectively an increase in burial efficiency, further accelerating the rate at which the oxygen source responds to decreases in pO_2.

Finally, the weathering of organic carbon increases with pO_2. As oxygen decreases in the rapid-respiration scenario, organic weathering falls by 40% even as pyrite and organic carbon burial increase, allowing redox balance to be achieved with less overall change in pO_2 than would be expected for a fixed sink.

3.2.4. Sensitivity to sulfate reduction

Sulfate reduction in the sediment is linear in the overlying SO_4^{2-} concentration. A ten-fold increase in the rate constant results in pO_2 of 1.1 PAL, compared to 0.4 PAL for a similar increase in the rate constant for aerobic respiration. Along with the feedbacks discussed above, several additional effects weaken the impact of sulfate reduction on the oxygen source, particularly as compared to aerobic respiration. First, elevated sulfide production results in additional pyrite burial, driving oceanic sulfate to 13 mM. This slows respiration such that S equilibrium is achieved with just a doubling of sulfate reduction, despite the ten-fold change in rate constant. Furthermore, pyrite formation is a transfer of electrons from one sedimentary sink to another, so the pyritized fraction of sulfide production (15%) is unimportant from a redox perspective.

3.2.5. Sensitivity to pyrite burial

Pyrite burial is modeled as an O_2-dependent fraction of the sulfide produced during sedimentary sulfate reduction. pO_2 stabilizes at 0.4 PAL if this fraction decreases from 20% at modern oxygen to a fixed 2%. Pyrite burial falls from 1.3 to 0.3 Tmol S yr^{-1}, limited to a five-fold decrease by the accumulation of sulfate (39 mM) and the subsequent acceleration of sulfide production. Oxygen decreases in response to this loss of source, raising organic carbon burial and reducing organic carbon weathering until equilibrium is re-achieved.

3.2.6. Sensitivity to sulfate burial

Direct burial of sulfate minerals is first order in sulfate concentration. A ten-fold increase in the rate constant reduces pO_2 to 0.9 PAL. More rapid burial draws sulfate down to 4 mM, resulting in equilibrium sulfate burial of 3.3 Tmol S yr^{-1}, increased from 2.3. This large S sink is balanced by slower sulfate reduction and pyrite burial, which induces a net decrease in oxygen source of 3.6 Tmol C yr^{-1}. pO_2 rises in compensation, raising burial efficiency and slowing weathering.

3.2.7. Sensitivity to pyrite weathering

The weathering of pyrite is a fixed flux in our model. To isolate the effect of this flux on pO_2, increases in pyrite oxidation are offset by decreases in sulfate weathering, such that the total flux of S to the ocean is unchanged. The entire sulfur flux is sourced from pyrite for a quadrupling of the weathering flux, which drives pO_2 to 0.5 PAL. This large electron source is partially offset by additional pyrite burial, which grows from 35% to 70% of sulfur burial in the low-oxygen ocean. 1.1 Tmol sulfate are still buried each year, however, so the exposure of purely pyritic S minerals is inconsistent on sufficiently long time scales. This should eventually reduce the size of the pyrite sink for oxygen, but we are unable to test this effect without a model for uplift and emplacement of sediments on the continents. 0.13 PAL oxygen is possible for a ten-fold increase in pyrite weathering, though this requires the total surface sulfur reservoir to increase by a factor of $\sim$3.

3.2.8. Sensitivity to organic carbon weathering

Organic carbon weathering scales with the square root of pO_2 in our model. A ten-fold increase in the rate constant reaches equilibrium at 0.75 PAL pO_2. Rapid weathering increases the size of the oxygen sink, but organic burial efficiency and hence the oxygen source rise in response as well, balancing at an 8-fold increase in weathering and an additional 21 Tmol organic C and 0.9 Tmol pyrite S buried annually.

3.2.9. Sensitivity to sedimentary phosphorus cycling

In our model, an oxygen-sensitive fraction of the P remineralized in the sedimentary is regenerated to the water column. At steady state, this loss must be exactly balanced by additional gross

burial of organic P. Therefore, any recycled P represents additional deposition and an effective increase in burial efficiency. As an extreme example, we can set the regenerated fraction to zero at all oxygen levels. This model stabilizes at 0.92 PAL, slowing respiration such that net organic burial remains 60% of gross deposition, despite a 5 Tmol C yr^{-1} reduction in the latter.

3.2.10. Sensitivity to mantle fluxes

Mantle electrons enter the ocean-atmosphere system as hydrothermal fluids, volcanic gases, and minerals along ridge flanks.

Oxidation of new crust is parameterized as an oxygen-sensitive weathering of ferrous iron. A ten-fold increase in the rate constant reduces pO_2 to 0.77 PAL. The large iron sink draws down oxygen until redox balance is achieved through rising organic burial, falling organic weathering, and a decrease in iron oxidation itself. As an alternative parameterization we can model crustal oxidation as independent of O_2, i.e. as fast enough to oxidize to completion at any oxygen level. In this case, a ten-fold increase in the exposure rate reduces pO_2 to 0.56 PAL.

A ten-fold increase in the flux of hydrothermal sulfide drives equilibrium pO_2 to 0.43 PAL. Though the sulfide is a large sink for oxygen, it also triples sulfur inputs to the ocean, which are balanced by an additional 6.5 Tmol pyrite S buried every year. This large additional source prevents oxygen from plunging to zero.

Volcanic outgassing releases many redox-sensitive species to the atmosphere; we represent changes in this flux simply as a scaling of CO_2 and sulfide inputs. Surprisingly, a ten-fold decrease in outgassing brings pO_2 down to 0.5 PAL, despite the smaller sulfide flux. pCO_2 stabilizes at 150 ppm due to the small carbon supply, halving the rate of phosphorus weathering. This loss of P input is a powerful lever on pO_2, as discussed below, resulting in lower oxygen.

3.2.11. Sensitivity to phosphorus input

The primary source of phosphorus is weathering of apatites. A ten-fold decrease in this term stabilizes pO_2 at 0.05 PAL. The small phosphorus supply supports less production, reducing organic deposition by a factor of five, such that the shuttle of P to the sediment can balance the smaller input, after allowing for P regeneration. The small gross organic flux reduces the oxygen source, and pO_2 falls; net burial efficiency rises by 40% in response, restoring equilibrium. The suboxic ocean exports organic particles very efficiently, and so only 10 Tmol C yr^{-1} primary production is needed to maintain the necessary burial.

3.3. Multiple steady states models for pO_2

When an arbitrary oxygen-sensitive P flux is included in the model, atmospheric O_2 is able to stabilize at *two* levels, converging to either a high or a low concentration depending on its initial state (Fig. 4); low pO_2 is achieved for sufficiently low initial concentrations of oxygen and sulfate. Existence of this behavior depends on the precise oxygen sensitivity of the P flux: a wide class of simple, smooth relationships produces two stable pO_2 levels. In particular, multiple steady states are possible when the positive feedback between P and oxygen becomes weak near the expected equilibrium pO_2 values (Kump et al., 2009). "Weak" variation is defined relative to the rate at which equilibrium pO_2 increases with an imposed P flux (Fig. 4, dotted line).

4. Discussion

4.1. The instability of a low oxygen atmosphere

Our Phanerozoic-tuned model always converges to a modern, high-oxygen state, even when it is initially anoxic and stripped of sulfate and phosphorus. This stability is driven by more efficient organic carbon and pyrite burial under low oxygen conditions (see also Section 4.4.1). For example, when this model is initialized with zero oxygen, the total annual O_2 source is 21 Tmol, three times the modern value and seven times the oxygen sink. The imbalance rapidly pumps oxygen into the system. As in earlier models (Berner and Canfield, 1989; Lasaga and Ohmoto, 2002; Bergman et al., 2004), this simple feedback is sufficient to explain the stability of Phanerozoic redox conditions. However, the feedback also prevents Proterozoic-like conditions from prevailing for more than a few million years. To achieve stability, a low-oxygen world must somehow limit growth in the oxygen source, despite slowed respiration and a P-driven lower-limit on the organic flux to the sediment.

4.2. Is the Black Sea an analog for the Proterozoic Ocean?

By providing a floor on organic carbon deposition, larger phosphorus inputs actually maintain higher levels of pO_2 (Fig. 2). This is a fundamental limitation in stabilizing a low-oxygen world, but may seem counter-intuitive in the context of modern eutrophic basins. The Black Sea, for example, is totally anoxic at depth precisely because phosphorus inputs through the Danube are large enough to support vigorous export production, which consumes all the oxygen in the poorly ventilated deep waters (Konolov and Murray, 2001).

Anoxic basins such as the Black Sea are poor models for global anoxia. They are coupled to a much larger well-oxygenated atmosphere/ocean, forming a highly oxidizing boundary condition. Therefore, these basins can bury organic carbon without significantly impacting pO_2, despite their high burial efficiencies (Arthur et al., 1994). Once decoupled from this essentially infinite reservoir, efficient burial would drive up pO_2, exacerbated by a slow-down in mineralization due to a loss of sulfate-rich Mediterranean water over the Bosporus sill (Ozsoy and Unluata, 1997). Ultimately pO_2 would rise until the slow Black Sea mixing oxygenated the deep and restored O_2 equilibrium.

To demonstrate this, we fix pO_2 in our model and add flows of oxygenated ocean water into the deep basin, and phosphorus-rich river water into the surface. Methanogenesis is included (following Section 2.5). Sure enough, this results in an anoxic deep basin (0 μM [O_2]), high phosphorus (20 μM [PO_4^{3-}]) and vigorous primary production (4000 Tmol C yr^{-1}, scaled to the surface area of the global ocean). When the sill overflow is shut off and the atmosphere is driven by the basin alone, the steady-state looks just like a smaller version of the modern global ocean with substantially higher P inputs and increased stratification: well oxygenated (80 μM), with moderate levels of deep water phosphorus (1.7 μM). The nutrient-rich, anoxic basin is possible specifically because it exchanges with an effectively infinite oxidized reservoir. High phosphorus levels therefore do not imply low oxygen in a global ocean. This distinction is critical in understanding how the modern phosphorus flux limits the sensitivity of pO_2 to changes in the redox system.

4.3. Mechanisms for a stable low oxygen atmosphere

As noted above, a low-oxygen world must limit growth in the oxygen source, despite more efficient burial of an organic flux maintained by phosphorus cycling. Coupled with a number of secondary negative feedbacks, this leaves pO_2 insensitive to most aspects of geochemical cycling. The sensitivity tests show that a reduction in the riverine phosphorus flux is by far the most powerful lever on pO_2, ruling out other mechanisms for a stable low-oxygen world.

4.3.1. Ballasting and burial mechanisms

Balance of the phosphorus budget leaves water-column carbon cycling irrelevant to pO_2, demonstrated by the insensitivity to settling rate and water column respiration. Any alteration to gross organic deposition perturbs the phosphorus budget, driving compensating changes in primary productivity to ensure the organic P sink balances inputs. This discounts the hypothesis of Logan et al. (1995), which proposes lower pre-Cambrian oxygen due to less efficient export of organic particles before the advent of ballasting fecal pellets.

4.3.2. Respiration-related mechanisms

One way to maintain modern burial efficiency at low oxygen is to invoke a compensating increase in the efficiency of respiration, such that remineralization rates themselves remain unchanged. The sensitivity of pO_2 to the rate constants for aerobic and anaerobic respiration show this can be successful in reducing oxygen levels. However, secondary negative feedbacks weaken the response, such that more than ten-fold changes to rate constants are required to stabilize oxygen at 0.1 PAL: an increase in the efficiency of pyrite burial at low oxygen (Berner and Westrich, 1985), a drop in organic carbon weathering (Chang and Berner, 1999), and a greater fraction of regenerated pore water P (Shaffer, 1986, Anderson et al., 2001), all conspire to limit the drop in pO_2. Changes of this scale cannot be justified by invoking, for example, the hypothesis of Kennedy et al. (2006). They argue that a difference in weathering products before the advent of land plants drove a seven-fold decrease in protective sorption relative today – much too small to achieve Proterozoic levels of oxygen.

4.3.3. Sink mechanisms

The simplest explanation for low pO_2 is a sufficiently large Proterozoic sink for oxygen. Fixed fluxes are the most powerful levers, but it is difficult to justify the order-of-magnitude changes required to explain Proterozoic oxygen. A doubling of present-day hydrothermal fluxes is possible for the Mesoproterozoic (Canfield, 2004; Kump and Barley, 2007). Pyrite weathering could have been 3–4 times greater if the Proterozoic surface sulfur reservoir were almost 100% pyrite, consistent with the thin distribution of Proterozoic evaporites (Grotzinger and Kasting, 1993), but this could only be maintained with increased pyrite burial.

4.3.4. Phosphorus-based mechanisms

Though organic carbon is efficiently buried in a low oxygen ocean, the net O_2 source need not grow if there is a compensating reduction in the gross flux of organic material to the seafloor. However, as the dominant P shuttle (Delaney, 1998), this flux must be large enough to balance P inputs.

This limitation would be lifted if mineral shuttling of phosphorus were much larger than today. Bjerrum and Canfield (2002) have proposed adsorption onto banded iron formations (BIFs) as a mechanism for suppressing phosphate. However, the lack of BIFs between 1.8 and 0.7 Ga (Holland, 1984) makes this an unlikely candidate for Proterozoic P control. Furthermore, adsorption is proportional to P concentration, so iron has a limited ability to remove phosphate from an anoxic ocean in which efficient organic export would limit deep-water nutrients. As shown in the sensitivity tests, even if the equivalent of the entire modern reactive iron flux is oxidized in open water, pO_2 cannot be maintained at less than 50% PAL.

Alternatively, the P budget would require less gross organic deposition if phosphorus inputs were smaller. Oxygen would decrease, maintaining net burial with a compensating increase in the burial efficiency of organic carbon and pyrite. As shown in Fig. 2, a ten-fold reduction in the riverine P flux stabilizes pO_2 at 0.1 PAL.

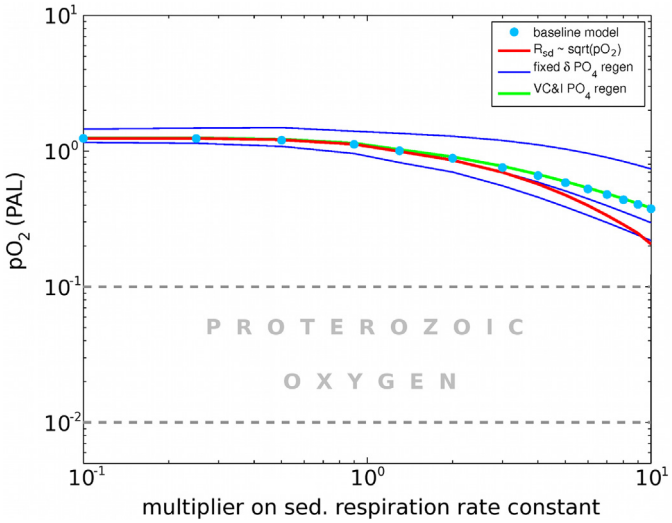

Fig. 3. Sensitivity of steady-state pO_2 to the rate constant on sedimentary respiration under different model configurations. Blue dots: baseline model with respiration rate linear in oxygen and O_2-sensitive diffusion of remineralized P (compare to curve 15 in Fig. 2). Red curve: respiration rate scales with square root of oxygen. Blue curves: diffusion of P is a fixed fraction of remineralization. Green curve: diffusion of P is an O_2-sensitive fraction of gross deposition.

A relationship between pO_2 and phosphorus input was identified in some earlier models (Lenton and Watson, 2004; Fennel et al., 2005), though these either did not include the burial efficiency feedback, or allowed it only near modern levels of oxygen. Relaxing this feedback makes it much less difficult to stabilize low oxygen. However, we find a relationship between pO_2 and phosphorus flux even when this stabilizing feedback is included. Of all the changes tested, a reduction in the riverine flux of bioavailable phosphorus requires the smallest change to drive the atmosphere to Proterozoic oxygen levels.

4.4. Sensitivity to model assumptions

The sensitivity tests discussed above assume the structure of our model is essentially correct, but it does include two controversial negative feedbacks: oxygen-dependent organic burial efficiency, and oxygen-dependent P regeneration. Here we consider the validity and importance of these assumptions.

4.4.1. Oxygen and organic carbon burial efficiency

Organic carbon burial efficiency has been shown to vary with oxygen in many environments. Along the Washington margin, Hedges et al. (1999) observe an increase in organic carbon content with decreasing oxygen penetration depth, which depends on bottom water O_2 (Cai and Sayles, 1996). This environment also has lower organic carbon content than the less oxic Mexican margin (Hartnett and Devol, 2003). Canfield (1993) finds a negative correlation between burial efficiency and bottom-water oxygen in a wide compilation of sediments, particularly at low sedimentation rates. Cowie et al. (1995) show that organic carbon contents are much higher below the oxygen penetration depth in the 100,000 year-old Madeira abyssal plain turbidite, allowing for integration over a very long period of alteration.

Though there is convincing evidence for an oxygen effect on organic burial efficiency, the exact relationship is unknown. Here we test an alternative parameterization in which remineralization scales with the square root of oxygen in the overlying water column. In this case, pO_2 is more sensitive to variations in the remineralization rate constant (Fig. 3). If Proterozoic remineralization were somehow ten times more efficient than today (Section 4.3.2), then the square root model predicts a 0.2 PAL atmosphere, while

the linear model gives 0.4 PAL. For a more modest doubling of the rate constant, both models stabilize at ~0.85 PAL. Therefore, we believe that our basic finding, of a weak relationship between pO_2 and the remineralization rate constant, is robust.

It should be stressed that our model couples pO_2 to oxic respiration, not to burial efficiency itself. This results in a weaker-than-linear scaling between oxygen levels and burial efficiency: even at zero oxygen, sulfate reduction ensures burial efficiency is not 100%. Indeed, we allow sulfate reduction to become more vigorous at lower oxygen levels, due to the possibility that sulfate reduction is limited in modern environments by the availability of the most labile carbon (Westrich and Berner, 1984).

4.4.2. Oxygen and phosphorus regeneration

Oxygen-dependent loss of pore water P has been documented in a compilation of sedimentary profiles (Colman and Holland, 2000), suggesting enhanced diffusion from sediments underlying low-oxygen waters. This could be due to shoaling of the iron redox boundary, where P can accumulate due to iron cycling (e.g. Sundby et al., 1992), as proposed by Shaffer (1986) for the Black Sea. There are few quantitative bounds on this relationship beyond a handful of observations by Filippelli (2002).

We can eliminate this oxygen-dependence by setting diffusive loss to a fixed fraction of remineralization. In the extreme case with no diffusive loss, pO_2 does become more responsive to changes in respiration rate constants (Fig. 3), stabilizing at 0.2 PAL for an implausible ten-fold increase. As the fixed fraction of P loss rises, the stable pO_2 value increases. Therefore, we believe our conclusion is robust: changes to sedimentary processes alone cannot explain Proterozoic oxygen levels.

Van Cappellen and Ingall (1994) have influentially argued that P is preferentially *remineralized* at low oxygen. Though their estimates for P loss have been revised downward by Anderson et al. (2001) after accounting for authigenic P minerals, we can test this model by setting P release to scale with organic deposition, rather than with remineralization. Most organic P is remineralized today, so this distinction makes almost no difference in our results (Fig. 3).

4.5. Biogeochemistry of the Proterozoic Ocean

A low oxygen atmosphere is only possible in our model if primary production is maintained at low levels through a reduction in inputs of the limiting nutrient. Independent of the mechanism for reducing nutrient fluxes, the Proterozoic must have been a period of limited productivity relative to today, with implications for the sulfur cycle, carbon isotopes and marine ecosystems.

We simulate a low-oxygen world by applying a 5-fold reduction in phosphorus inputs to the model with a Mesoproterozoic solar luminosity and no evaporite weathering (Figure S2). In this simulation primary production is several hundred times less than today, about 10 Tmol C yr^{-1}, but is exported and buried more than ten times more efficiently. The net result is a ratio of organic to total carbon burial around 0.05. This is significantly less than the carbon isotopic record suggests (Canfield, 2004), though traditional C isotope mass balance models may be inadequate (Schrag et al., 2013). Without extensive water column respiration, deep-water P concentration falls to 0.02 μM. Phosphate-poor upwelling and efficient export starves the photic zone of nutrients, maintaining low productivity. River-borne P accounts for nearly a third of primary production, compared to a few percent today (Dunne et al., 2007). Therefore, it is possible Proterozoic productivity was redistributed primarily along coastal environments and particularly near estuaries. Unfortunately we cannot explore this hypothesis in a 1D ocean model.

With so little production, global nitrogen demand would have been hundreds of times lower than today, largely met by inorganic sources of fixed nitrogen such as lightning strikes, which make up 2% of modern total nitrogen fixation (Galloway et al., 2004). This conclusion depends only on the need for low productivity to compensate for the increased burial efficiency of anoxic sediments, rather than on the particular simulation discussed here. Therefore, limitation by nitrogen itself (Fennel et al., 2005) or by trace metal stress on nitrogen fixers (Planavsky et al., 2010) is unlikely at a global scale, consistent with our assumption of phosphorus limitation.

Seawater sulfate is reduced to 3 mM in our low-oxygen simulation, in agreement with evidence from a number of Mesoproterozoic basins (Poulton and Canfield, 2011). Sulfate is drawn down by more than a doubling of pyrite burial, driven by increased sulfate reduction and inefficient reoxidation of sulfide. A predominantly pyritic sink for sulfur is consistent with the sulfur isotopic record (Canfield, 2004) and the scarcity of Proterozoic evaporites (Grotzinger and Kasting, 1993). Without sulfate burial, pyrite would make up the bulk of exposed sulfur minerals; for simplicity we assume 100% of weathered sulfur was pyrite. This is an extreme end member: at smaller fractions the net sulfur cycle is a smaller source of electrons, and a larger reduction in phosphorus is necessary to maintain low oxygen.

4.6. Multiple steady states: an oxygen-dependent "iron trap" for phosphorus

Any mechanism that limits phosphorus inputs and primary production during the Proterozoic is sufficient to explain the low-oxygen atmosphere. This mechanism could take several forms: oxidation of the atmosphere could be due to an external nutrient forcing that evolves through discrete stages. Alternatively, pO_2 may be a truly multiple steady state system, which will remain it its initial low oxygen state until forced into the high oxygen regime by a sufficiently large perturbation. Here we pursue one possible multiple equilibrium solution, motivated by the existence of a major perturbation in the Neoproterozoic Snowball Earth events.

Our sensitivity tests show that a multiple state model requires a feedback that maintains lower phosphorus in lower-oxygen rivers. Apatite dissolution, the primary source of fluvial P (Filippelli, 2002), is not an oxidative process, so the feedback cannot involve phosphorus weathering itself. The geochemistry of iron, however, will be greatly affected by lower O_2 in the atmosphere. This change may have played an important part in limiting P delivery to rivers through scavenging by iron oxides.

Phosphate is commonly found sorbed to iron oxides in river colloids. Adsorption is greatest when ferrous iron oxidizes in solution with dissolved anions, as in anoxic groundwater outflows (Mayer and Jarrell, 2000). In laboratory experiments (Mayer and Jarrell, 2000), such "co-precipitation" raises the particulate P:Fe ratio by a factor of 10 compared to direct addition of ferric iron to solution. This may be due to the high surface area of the colloidal oxides before particle aggregation (Fuller et al., 1993), or to the high surface area of ferrihydrite before crystallization (Mayer and Jarrell, 2000). Today, iron liberated during weathering is typically oxidized immediately, before eroding into groundwaters. In the weathering environment of a 0.1 PAL atmosphere, the kinetics of iron oxidation would be 10 times slower than today (Millero et al., 1987b), resulting in significant transport of ferrous iron out of soils, and subsequent oxidation in rivers and estuaries. The efficiency of P scavenging would greatly increase, limiting bioavailable P. There is evidence for this effect in modern environments: while iron particles in rivers have P:Fe ratios well below 0.1 (Fox, 1990, 1991), precipitates in eutrophic lakes (Buffle et al., 1989) and hydrothermal plumes (Feely et al., 1998) have ratios greater

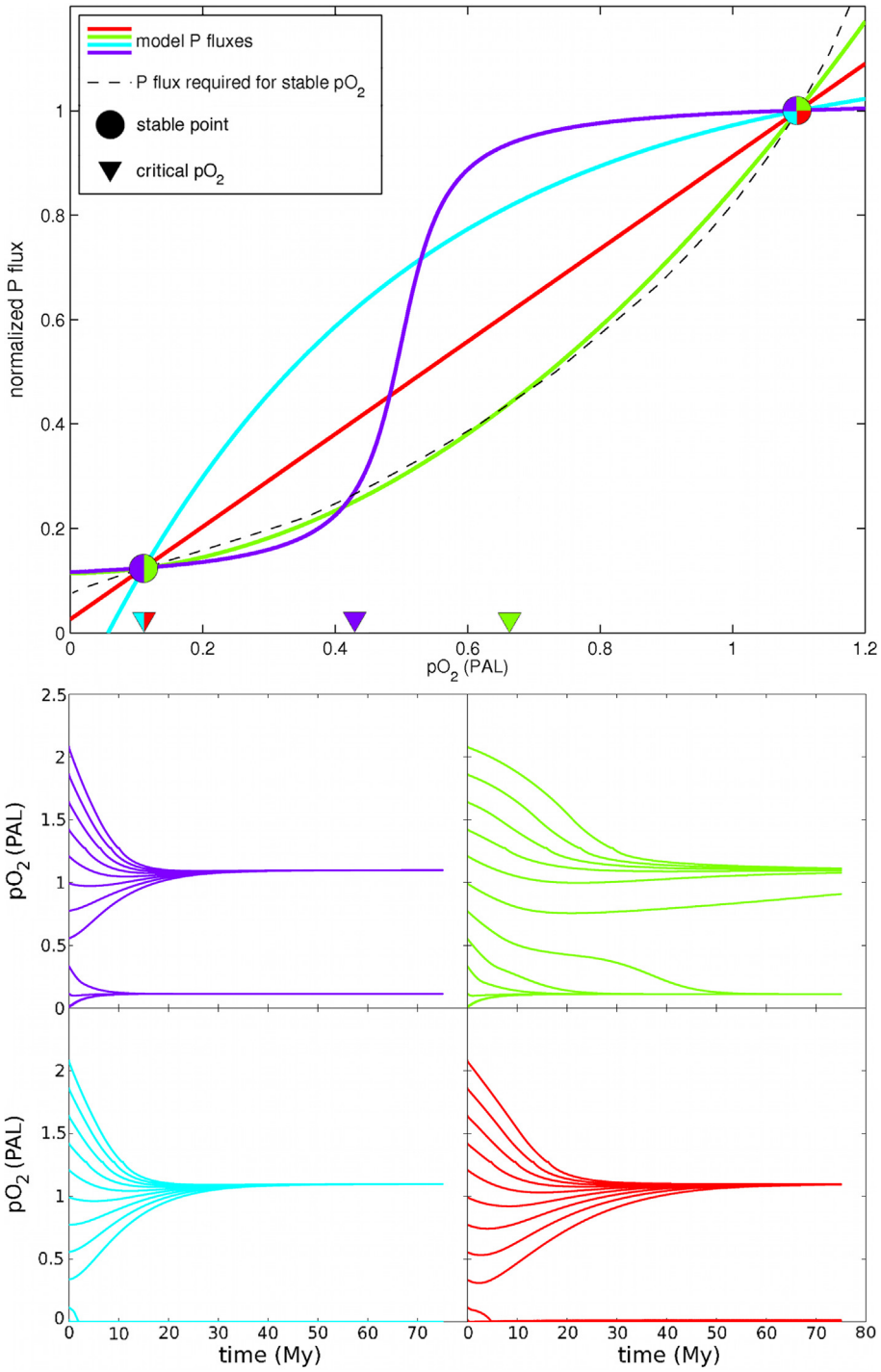

Fig. 4. Models of multiple stable pO_2 levels. Top: Four models of an oxygen-sensitive input of phosphate. The dashed line shows the P input required to maintain pO_2 at a given level. Stable equilibria are marked with circles, unstable equilibria with triangles. Bottom: evolution of pO_2 from various initial conditions for each of the P input models. The green and purple models give multiple steady states.

than 0.25. This mechanism does require permanent burial of iron-bound phosphorus, either through rapid sedimentation in estuaries, or precipitation of secondary P minerals.

4.7. Testing the iron trap

The iron-trap mechanism is only plausible if it can explain a 5-fold reduction in phosphorus without oxidizing more iron than is available today: the reactive iron load in modern rivers, overwhelmingly in ferric particulates, ranges from 100 to >500 μM (Poulton and Raiswell, 2002). If co-precipitation forms particles with an excess P:Fe ratio of α, then the ferrous iron concentration required for an x-fold reduction is given by:

$$\left[Fe^{2+}\right] = \alpha^{-1}[P]_{riv}(1 - 1/x)$$

The appropriate P concentration is probably much larger than the instantaneously dissolved load, since loosely bound phosphorus may account for two-thirds of the bioavailable supply (Froelich, 1988; Benitez-Nelson, 2000). Using three times the average dissolved phosphate concentration in modern rivers (0.6 μM, Carpenter and Bennett, 2011), and $\alpha = 0.45$ (Mayer and Jarrell, 2000), we

find 2–4 μM of ferrous iron must have been oxidized in Proterozoic rivers, just a few percent of the modern load.

Phosphorus adsorption is affected by a number of other factors, notably pH. Preferential adsorption occurs in more acidic water (Fuller et al., 1993) favoring our hypothesis given the high pCO_2 required to offset the faint Proterozoic sun. However, other important factors, such as silica and organic ligand concentration, and the many determinants of oxide mineralogy, are difficult to assess for ancient rivers. Furthermore, the P:Fe ratios observed in laboratory experiments are typically generated with high initial P loads, and therefore the calculation above may underestimate the necessary iron load.

Nevertheless, we expect the supply of bioavailable phosphorus to increase with rising pO_2. Iron minerals have maximum adsorption capacities that are reached at high ferrous iron concentration (Gunnars et al., 2002), so P uptake is likely less responsive to pO_2 at lower levels. This corresponds to the type of phosphorus–oxygen relationships that produce two steady states in our model (Fig. 4). More specifically, iron dynamics must produce a P vs. O_2 relationship that crosses the oxygen stability curve (Fig. 4), with smaller slope, at 1 and 0.1 PAL.

Our multiple-steady state model is the first quantitative hypothesis that explains both the modern and Proterozoic atmosphere. It also has important implications for the step-like rise in pO_2 in the Neoproterozoic. A large, transient fluctuation in Neoproterozoic oxygen, perhaps driven by extreme glaciations, could have reduced co-precipitation of iron and phosphorus, driving up the riverine P flux and ultimately forcing the redox cycle into its high production, high oxygen regime. No fundamental innovation in the geochemical or biological system is required to explain the transition. The Proterozoic atmosphere had merely to wait for a large enough perturbation to drive it into a stable, high-oxygen state.

5. Conclusions

Our simple model for atmospheric pO_2 is stabilized by oxygen-sensitive organic carbon and pyrite burial. Under low oxygen conditions, more efficient burial drives O_2 back to modern-day levels. To maintain a low oxygen equilibrium condition, we find the only plausible parameter change in our simple model is a feedback that reduces riverine phosphorus inputs under low oxygen conditions, preventing the phosphorus from stimulating new photosynthesis. Such a relationship compensates for higher burial efficiency with a smaller shuttle of organic material to the sediment. Therefore, multiple steady states in atmospheric oxygen requires some new positive feedback linking increased pO_2 to increased phosphorus inputs.

We identify one possible mechanism for this feedback involving more efficient nutrient scavenging by iron under more reduced conditions. In a low oxygen atmosphere, rivers would carry more ferrous iron because the kinetics of iron oxidation are slower. Slow oxidation of iron in solution in rivers and estuaries more efficiently scavenges phosphorus, consistent with experimental evidence. Simple parameterizations of this feedback results in a model with two equilibrium states for oxygen, a low oxygen state with pO_2 of a few percent PAL, potentially consistent with Proterozoic conditions, and a high oxygen state with pO_2 near 1 PAL, consistent with the Phanerozoic.

Acknowledgements

We thank David Johnston, John Higgins, Itay Halevy and Wil Leavitt for their suggestions. The manuscript was improved with comments from Lee Kump and an anonymous reviewer. This work was supported by NASA Headquarters under the NASA Earth and Space Science Fellowship Program Grant NNX11AP89H.

Appendix A. Supplementary material

Supplementary material related to this article can be found online at http://dx.doi.org/10.1016/j.epsl.2013.11.049.

References

Anbar, A., Knoll, A., 2002. Proterozoic ocean chemistry and evolution: a bioinorganic bridge?. Science 297, 1137–1142.
Anbar, A., Duan, Y., Lyons, T., Arnold, G., Kendall, B., Creaser, R., Kaufman, A., Gordon, G., Scott, C., Garvin, J., Buick, R., 2007. A whiff of oxygen before the great oxidation event?. Science 317, 1903–1906.
Anderson, L., Delaney, M., Faul, K., 2001. Carbon to phosphorus ratios in sediments: Implications for nutrient cycling. Glob. Biogeochem. Cycles 15, 65–79.
Armstrong, R., Lee, C., Hedges, J., Honjo, S., Wakeham, S., 2002. A new, mechanistic model for organic carbon fluxes in the ocean based on the quantitative association of POC with ballast minerals. Deep-Sea Res., Part 2, Top. Stud. Oceanogr. 49, 219–236.
Arthur, M., Dean, W., Neff, E., Hay, B., King, J., Jones, G., 1994. Varve calibrated records of carbonates and organic carbon accumulation over the last 2000 years in the Black Sea. Glob. Biogeochem. Cycles 8, 195–217.
Benitez-Nelson, C., 2000. The biogeochemical cycling of phosphorus in marine systems. Earth-Sci. Rev. 51, 109–135.
Bergman, N., Lenton, T., Watson, A., 2004. COPSE: A new model of biogeochemical cycling over Phanerozoic time. Am. J. Sci. 304, 397–437.
Berner, R., 2006. GEOCARBSULF: A combined model for Phanerozoic atmospheric O_2 and CO_2. Geochim. Cosmochim. Acta 70, 5653–5664.
Berner, R., Canfield, D., 1989. A new model for atmospheric oxygen over Phanerozoic time. Am. J. Sci. 289, 333–361.
Berner, R., Westrich, J., 1985. Bioturbation and the early diagenesis of carbon and sulfur. Am. J. Sci. 285, 193–206.
Bjerrum, C., Canfield, D., 2002. Ocean productivity before 1.9 Gyr ago limited by phosphorus adsorption onto iron oxides. Nature 417, 159–162.
Buffle, J., De Vitre, R., Perret, D., Leppard, G., 1989. Physico-chemical characteristics of a colloidal iron phosphate species formed at the oxic–anoxic interface of a eutrophic lake. Geochim. Cosmochim. Acta 53, 399–408.
Cai, W., Sayles, F., 1996. Oxygen penetration depths and fluxes in marine sediments. Mar. Chem. 52, 123–131.
Canfield, D., 1993. Organic matter oxidation in marine sediments. In: Wollast, R., Mackenzie, F., Chou, L. (Eds.), Biogeochemical Cycles and Global Change. Springer, Berlin, pp. 333–363.
Canfield, D., 2004. The evolution of the earth surface sulfur reservoir. Am. J. Sci. 304, 839–861.
Canfield, D., Teske, A., 1996. Late Proterozoic rise in atmospheric oxygen concentration inferred from phylogenetic and sulphur-isotopes studies. Nature 382, 127–132.
Capone, D., Kiene, R., 1988. Comparison of microbial dynamics in marine and freshwater sediments: Contrasts in anaerobic carbon catabolism. Limnol. Oceanogr. 33, 725–749.
Carpenter, S., Bennett, E., 2011. Reconsideration of the planetary boundary for phosphorus. Environ. Res. Lett. 6.
Catling, D., Zahnle, K., McKay, C., 2001. Biogenic methane, hydrogen escape, and the irreversible oxidation of the early earth. Science 293, 839–843.
Chang, S., Berner, R., 1999. Coal weathering and the geochemical carbon cycle. Geochim. Cosmochim. Acta 63, 3301–3310.
Colman, A., Holland, H., 2000. The global diagenetic flux of phosphorus from marine sediments to the oceans: redox sensitivity and the control of atmospheric oxygen levels. In: Glenn, C., Lucas, J., Prevot-Lucas, L. (Eds.), Marine Authigenesis: From Global to Microbial. In: SEMP Spec. Pub., vol. 66, pp. 53–75.
Cowie, G., Hedges, J., Prahl, F., Lange, G., 1995. Elemental and major biogeochemical changes across an oxidation front in a relict turbidite: An oxygen effect. Geochim. Cosmochim. Acta 59, 33–46.
Crowe, S., Katsev, S., Leslie, K., Sturm, A., Magen, C., Nomosatryo, S., Pack, M., Kessler, J., Reeburgh, W., Roberts, J., Gonzalez, L., Haffner, G., Mucci, A., Sundby, B., Fowle, D., 2011. The methane cycle in ferruginous Lake Matano. Geobiology 9, 61–78.
Dahl, T., Hammarlund, E., Anbar, A., Bond, D., Gill, B., Gordon, G., Knoll, A., Nielsen, A., Schovsbo, N., Canfield, D., 2010. Devonian rise in atmospheric oxygen correlated to the radiations of terrestrial plants and large predatory fish. Proc. Natl. Acad. Sci. USA 107, 17911–17915.
Delaney, M., 1998. Phosphorus accumulation in marine sediments and the oceanic phosphorus cycle. Glob. Biogeochem. Cycles 12, 563–572.
DeVries, T., Deutsch, C., Primeau, F., Chang, B., Devol, A., 2012. Global rates of water-column denitrification derived from nitrogen gas measurements. Nat. Geosci. 5, 547–550.
Dunne, J., Sarmiento, J., Gnanadesikan, A., 2007. A synthesis of global particle export from the surface ocean and cycling through the ocean interior and on the seafloor. Glob. Biogeochem. Cycles 21.
Elderfield, H., Schultz, A., 1996. Mid-ocean ridge hydrothermal fluxes and the chemical composition of the ocean. Annu. Rev. Earth Planet. Sci. 24, 191–224.

Feely, R., Trefry, J., Lebon, G., German, C., 1998. The relationship between P/Fe and V/Fe ratios in hydrothermal precipitates and dissolved phosphate in seawater. Geophys. Res. Lett. 25, 2253–2256.
Fennel, K., Follows, M., Falkowski, P., 2005. The co-evolution of the nitrogen, carbon and oxygen cycles in the Proterozoic ocean. Am. J. Sci. 305, 526–545.
Filippelli, G., 2002. The global phosphorus cycle. Rev. Mineral. Geochem. 48, 391–425.
Fox, L., 1990. Geochemistry of dissolved phosphate in the Sepik River and Estuary, Papua, New Guinea. Geochim. Cosmochim. Acta 54, 1019–1024.
Fox, L., 1991. Phosphorus chemistry in the tidal Hudson River. Geochim. Cosmochim. Acta 55, 1529–1538.
Froelich, P., 1988. Kinetic control of dissolved phosphate in natural rivers and estuaries: A primer on the phosphate buffer mechanism. Limnol. Oceanogr. 22, 649–668.
Fuller, C., Davis, J., Waychunas, G., 1993. Surface chemistry of ferrihydrite: Part 2. Kinetics of arsenate adsorption and coprecipitation. Geochim. Cosmochim. Acta 57, 2271–2282.
Galloway, J., Dentener, F., Capone, D., Boyer, E., Howarth, R., Seitzinger, S., Asner, G., Cleveland, C., Green, P., Holland, E., Karl, D., Michaels, A., Porter, J., Townsend, A., Vörösmarty, C., 2004. Nitrogen cycles: past, present, and future. Biogeochemistry 70, 153–226.
Goldblatt, C., Lenton, T., Watson, A., 2006. Bistability of atmospheric oxygen and the Great Oxidation. Nature 443, 683–686.
Grotzinger, J., Kasting, J., 1993. New constraints on Precambrian Ocean composition. J. Geol. 101, 235–243.
Gunnars, A., Blomqvist, S., Johansson, P., Andersson, C., 2002. Formation of Fe(III) oxyhydroxide colloids in freshwater and brackish seawater, with incorporation of phosphate and calcium. Geochim. Cosmochim. Acta 66, 745–758.
Habicht, K., Gade, M., Thamdrup, B., Berg, P., Canfield, D., 2002. Calibration of sulfate levels in the Archean ocean. Science 298, 2372–2374.
Halevy, I., Peters, S., Fischer, W., 2012. Sulfate burial constraints on the Phanerozoic sulfur cycle. Science 337, 331–334.
Hartnett, G., Devol, A., 2003. Role of a strong oxygen-deficient zone in the preservation and degradation of organic matter: A carbon budget for the continental margins of northwest Mexico and Washington State. Geochim. Cosmochim. Acta 67, 247–264.
Hedges, J., Keil, R., 1995. Sedimentary organic matter preservation: an assessment and speculative synthesis. Mar. Chem. 49, 81–115.
Hedges, J., Hu, F.S., Devol, A., Hartnett, H., Tsamakis, E., Keil, R., 1999. Sedimentary organic matter preservation: a test for selective degradation under oxic conditions. Am. J. Sci. 299, 529–555.
Hoffman, P., Schrag, D., 2002. The snowball Earth hypothesis: testing the limits of global change. Terra Nova 14, 129–155.
Holland, H., 1984. The Chemical Evolution of the Atmosphere and Oceans. Princeton University Press, Princeton.
Ingvorsen, K., Zehnder, A., Jorgensen, B., 1984. Kinetics of sulfate and acetate uptake by desulfobacter postgatei. Appl. Environ. Microbiol. 47, 403–408.
Jorgensen, B., Weber, A., Zopfi, J., 2001. Sulfate reduction and anaerobic methane oxidation in Black Sea sediments. Deep-Sea Res., Part 1, Oceanogr. Res. Pap. 48, 2097–2120.
Kennedy, M., Droser, M., Mayer, L., Pevear, D., Mrofka, D., 2006. Late Precambrian oxygenation; inception of the clay mineral factory. Science 311, 1446–1449.
Konovalov, S., Murray, J., 2001. Variations in the chemistry of the Black Sea on a time scale of decades (1960–1995). J. Mar. Syst. 31, 217–243.
Kump, L., 2008. The rise of atmospheric oxygen. Nature 451, 277–278.
Kump, L., Barley, M., 2007. Increased subaerial volcanism and the rise of atmospheric oxygen 2.5 billion years ago. Nature 1033–1036.
Kump, L., Garrels, R., 1986. Modeling atmospheric O_2 in the global sedimentary redox cycle. Am. J. Sci. 286, 337–360.
Kump, L., Kasting, J., Barley, M., 2001. Rise of the atmospheric oxygen and the "upside-down" Archean mantle. Geochem. Geophys. Geosyst. 2.
Kump, L., Kasting, J., Crane, R., 2009. The Earth System, 3rd ed. Prentice Hall.
Lasaga, A., Ohmoto, H., 2002. The oxygen geochemical cycle: Dynamics and stability. Geochim. Cosmochim. Acta 66, 361–381.
Lenton, T., Watson, A., 2004. Biotic enhancement of weathering, atmospheric oxygen and carbon dioxide in the Neoproterozoic. Geophys. Res. Lett. 31.
Logan, G., Hayes, J., Hieshima, G., Summons, R., 1995. Terminal Proterozoic reorganization of biogeochemical cycles. Nature 376, 53–56.
Martens, C., Klump, J., 1984. Biogeochemical cycling in an organic-rich coastal marine basin 4. An organic budget for sediments dominated by sulfate reduction and methanogenesis. Geochim. Cosmochim. Acta 48, 1987–2004.
Mayer, T., Jarrell, W., 2000. Phosphorus sorption during iron(II) oxidation in the presence of dissolved silica. Water Res. 34, 3949–3956.
Millero, F., Hubinger, S., Fernandez, M., Garnett, S., 1987a. Oxidation of H_2S in seawater as a function of temperature, pH, and ionic strength. Environ. Sci. Technol. 21, 439–443.
Millero, F., Sotolongo, S., Izaguirre, M., 1987b. The oxidation kinetics of Fe(II) in seawater. Geochim. Cosmochim. Acta 51, 793–801.
Muller-Karger, F., Varela, R., Thunell, R., Luerssen, R., Hu, C., Walsh, J., 2005. The importance of continental margins in the global carbon cycle. Geophys. Res. Lett. 32.
Özsoy, E., Ünlüata, Ü., 1997. Oceanography of the Black Sea: a review of some recent results. Earth-Sci. Rev. 42, 231–272.
Pavlov, A., Kasting, J., 2000. Mass-independent fractionation of sulfur isotopes in Archean sediments: strong evidence for an anoxic Archean atmosphere. Astrobiology 2, 27–41.
Planavsky, N., Rouxel, O., Bekker, A., Lalonde, S., Konhauser, K., Reinhard, C., Lyons, T., 2010. The evolution of the marine phosphate reservoir. Nature 467, 1088–1090.
Poulton, S., Canfield, D., 2011. Ferruginous conditions a dominant feature of the ocean through Earth's history. Elements 7, 107–112.
Poulton, S., Raiswell, R., 2002. The low-temperature geochemical cycle of iron: from continental fluxes to marine sediment deposition. Am. J. Sci. 302, 774–805.
Rye, R., Holland, H., 1998. Paleosols and the evolution of atmospheric oxygen: a critical review. Am. J. Sci. 298, 621–672.
Sarmiento, J., Gruber, N., 2006. Ocean Biogeochemical Dynamics. Princeton University Press, Princeton.
Schrag, D., Higgins, J., Macdonald, F., Johnston, D., 2013. Authigenic carbonate and the history of the global carbon cycle. Science 339, 540–543.
Scott, A., Glasspool, I., 2006. The diversification of Paleozoic fire systems and fluctuations in atmospheric oxygen concentration. Proc. Natl. Acad. Sci. USA 103, 10861–10865.
Shaffer, G., 1986. Phosphate pumps and shuttles in the Black Sea. Nature 321, 515–517.
Sundby, B., Gobeil, C., Silverberg, N., Mucci, A., 1992. The phosphorus cycle in coastal marine sediments. Limnol. Oceanogr. 37, 1129–1145.
Tyrrell, T., 1999. The relative influences of nitrogen and phosphorus on oceanic primary production. Nature 400, 525–531.
Van Cappellen, P., Ingall, E., 1994. Benthic phosphorus regeneration, net primary production, and ocean anoxia: A model of the coupled marine and biogeochemical cycles of carbon and phosphorus. Paleoceanography 9, 677–692.
Walker, J., Hays, B., Kasting, J., 1981. J. Geophys. Res. 86, 9776–9782.
Wang, Y., Van Cappellen, P., 1996. A multicomponent reactive transport model of early diagenesis: Application of redox cycling in coastal marine sediments. Geochim. Cosmochim. Acta 60, 2993–3014.
Westrich, J., Berner, R., 1984. The role of sedimentary organic matter in bacterial sulfate reduction: the G model tested. Limnol. Oceanogr. 29, 236–249.